iScience

Article

CRISPR/Cas9-mediated SHP-1-knockout T cells combined with simvastatin enhances anti-tumor activity in humanized-PDX HCC model

Graphical abstract

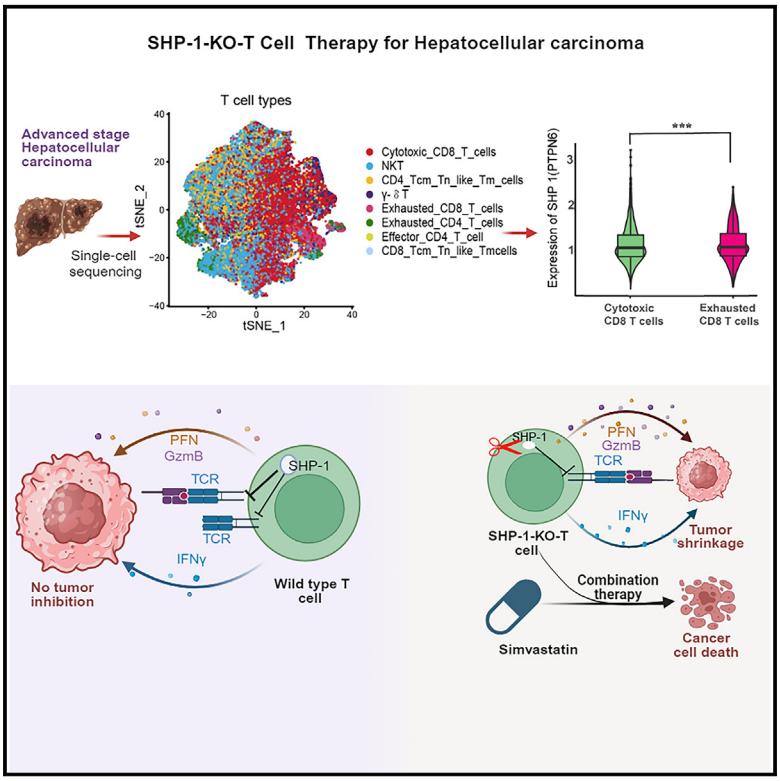

Highlights

- CRISPR-engineered SHP-1-KO CD8$^+$ T cells overcome immunosuppression in HCC models
- SHP-1 ablation enhances TEM cytotoxicity via IFN-γ/Granzyme B *in vitro* and PDX
- Simvastatin synergizes with SHP-1-KO T cells to amplify anti-HCC efficacy

Authors

Huaping Liu, Wu Ge, Xiaoping Yu, ..., Hailan Li, Xiaoqian Ma, Wei Wang

Correspondence

mxq8933@gmail.com (X.M.), wang_w@csu.edu.cn (W.W.)

In brief

Natural sciences; Biological sciences; Systems biology; Cancer systems biology; Cancer

Liu et al., 2025, iScience *28*, 112266
April 18, 2025
https://doi.org/10.1016/j.isci.2025.112266

CellPress

iScience

CellPress
OPEN ACCESS

Article

CRISPR/Cas9-mediated SHP-1-knockout T cells combined with simvastatin enhances anti-tumor activity in humanized-PDX HCC model

Huaping Liu,[1,2,3] Wu Ge,[1,3] Xiaoping Yu,[2] Jianwei Luo,[1,3] Juan Zhang,[1,3] Min Yang,[1,3] Lu Cao,[1,3] Yangnan Zhang,[4] Ruike Wang,[4] Cejun Yang,[1,3] Pei Li,[1,3] Mengyu Tian,[1,3] XiaoPei Peng,[1,3] Lei Peng,[1,3] Di Wu,[1,3] Muqi Liu,[1,3] Qi Liang,[1] Shengwang Zhang,[1] Wei Li,[1,3] Pengfei Rong,[1,3,5] Hailan Li,[6] Xiaoqian Ma,[1,3,5,*] and Wei Wang[1,3,5,7,*]

[1]Department of Radiology, the 3rd Xiangya Hospital of Central South University, Changsha, Hunan, China
[2]Department of Radiology, Hunan Cancer Hospital and the Affiliated Cancer Hospital of Xiangya School of Medicine, Central South University, Changsha, Hunan, China
[3]The Institute for Cell Transplantation and Gene Therapy, Central South University, Changsha, Hunan, China
[4]Xiangya School of Medicine, Central South University, Changsha, Hunan, China
[5]Molecular Imaging Research Center of Central South University, Changsha, Hunan, China
[6]Department of Radiology, Hunan Provincial People's Hospital, The First Affiliated Hospital of Hunan Normal University
[7]Lead contact
*Correspondence: mxq8933@gmail.com (X.M.), wang_w@csu.edu.cn (W.W.)
https://doi.org/10.1016/j.isci.2025.112266

SUMMARY

Hepatocellular carcinoma (HCC) resists immunotherapy due to its immunosuppressive microenvironment. Sarcoma homology 2 domain-containing protein tyrosine phosphatase-1 (SHP-1) inhibits T cell receptor signaling, and its pharmacological inhibition is limited by poor selectivity and membrane permeability. Here, we generated CRISPR-edited SHP-1-knockout (KO) $CD8^+$ T cells to enhance adoptive therapy against HCC. Single-cell RNA sequencing of HCC patient T cells revealed elevated SHP-1 in exhausted subsets. SHP-1-KO T cells exhibited increased effector memory T cells (TEM) proportions and enhanced IFN-γ/Granzyme B/perforin secretion, improving cytotoxicity against HCC lines. In humanized PDX models, SHP-1-KO T cells demonstrated superior tumor-killing activity. Transcriptomics identified upregulated lipid metabolism pathways, with HMGCR as a hub gene. Combining SHP-1-KO T cells with simvastatin (HMGCR inhibitor) synergistically amplified anti-HCC efficacy. This study proposes a dual strategy combining SHP-1-targeted cell therapy and metabolic modulation to overcome immunotherapy resistance, offering a translatable approach for HCC treatment.

INTRODUCTION

Hepatocellular carcinoma (HCC) is the most common type of primary liver cancer representing a significant global health challenge. The incidence of HCC is projected to reach approximately one million cases annually by 2025.[1–3] Despite advancements in cancer treatments, including targeted and immunotherapies, the clinical response rates remain low, with only 15–20% of patients with HCC experiencing objective responses.[4] This limited efficacy is largely due to the immunosuppressive tumor microenvironment, characterized by various inhibitory signals, ligands, metabolic factors, and compounds that impair the functionality of $CD8^+$ T cells, leading to their exhaustion.

Given the critical role of the immune system in combating cancer, enhancing the anti-tumor activity of T cells presents a promising therapeutic strategy. In particular, sarcoma homology 2 domain-containing protein tyrosine phosphatase-1 (SHP-1) inhibits T cell receptor (TCR) signaling, limiting T cell reactivity.[5,6] SHP-1 dephosphorylates key proteins in the TCR pathway, such as the TCR-ζ chain, lymphocyte-specific protein tyrosine kinase (LCK), zeta-chain-associated protein kinase 70 (ZAP70), Vav, and phosphoinositide 3-kinase (PI3K). Accordingly, targeting SHP-1 to reduce its inhibitory effects on T cells has been proposed as a potential cancer treatment strategy.

SHP-1-deficient T cells exhibit enhanced anti-tumor activity due to more stable and persistent synapses with antigen-presenting cells and increased proliferative responses.[7–10] However, the clinical application of SHP-1 inhibitors has been limited by selectivity and membrane permeability issues, leading to suboptimal anti-tumor effects and adverse reactions.[11,12] Thus, developing a more efficient and safer SHP-1-targeting strategy is imperative.

This study used CRISPR/Cas9 gene editing technology to knock out SHP-1 in activated T cells with an aim to improve their anti-tumor activity in HCC. By employing patient-derived xenograft (PDX) models, the efficacy of SHP-1-KO T cells was validated in a clinically relevant setting. Furthermore, the potential synergistic effects of combining SHP-1-KO T cells with

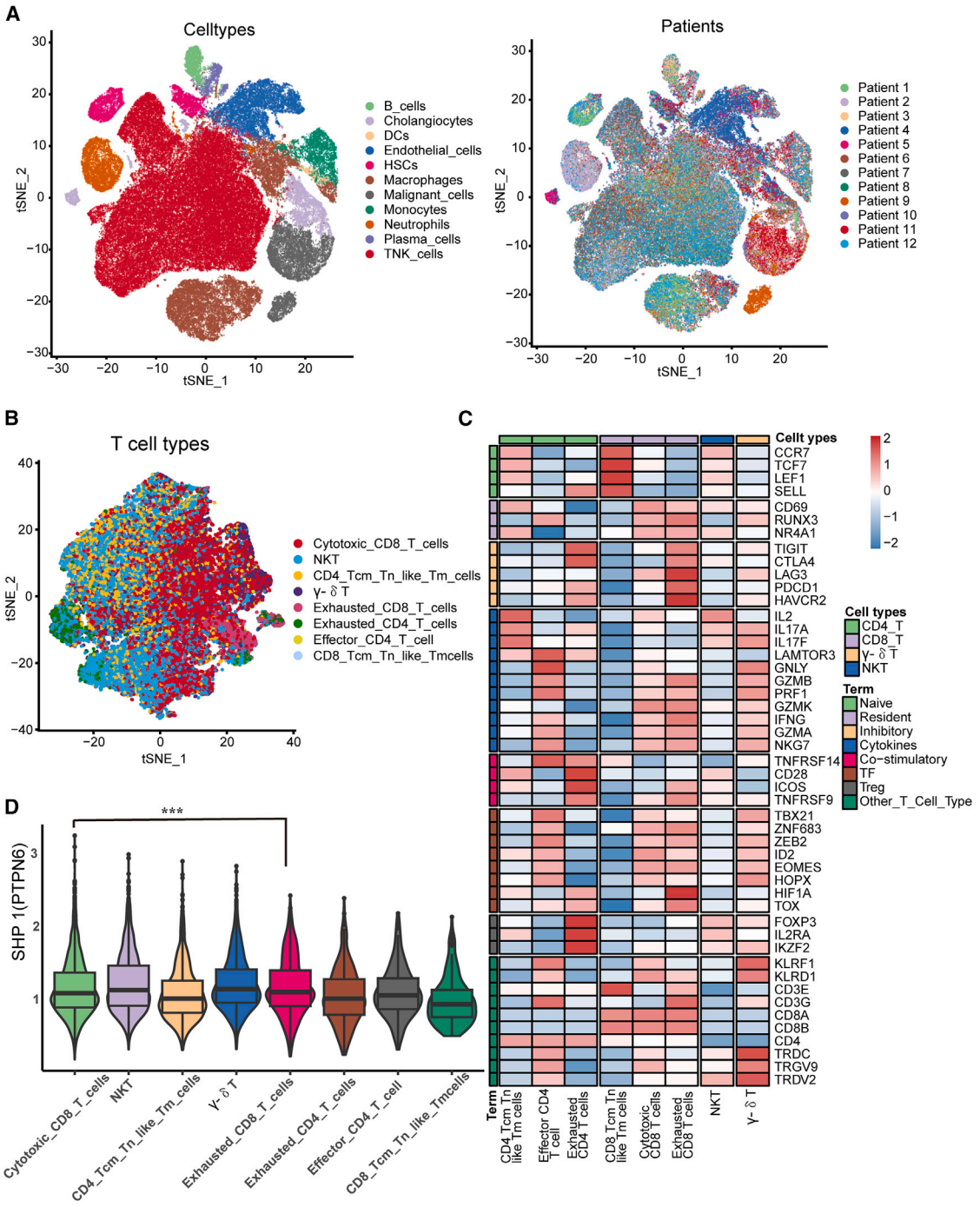

Figure 1. Single-cell RNA sequencing (scRNA-seq) profiling of intratumoral T cell SHP-1 expression in advanced HCC

(A) T-distributed stochastic neighbor embedding (t-SNE) plot, showing the annotation and color codes for cell types in the advanced HCC ecosystem. The number of patients is provided in the figure.

(B) t-SNE plot showing the defined T cell subsets.

(C) Heatmap showing the expression of marker genes in the indicated T cell types.

(D) Violin plot showing the expression of SHP1 in T cell subsets. ***$p < 0.001$, as assessed using a one-way analysis of variance with Tukey's multiple comparisons post hoc test (D).

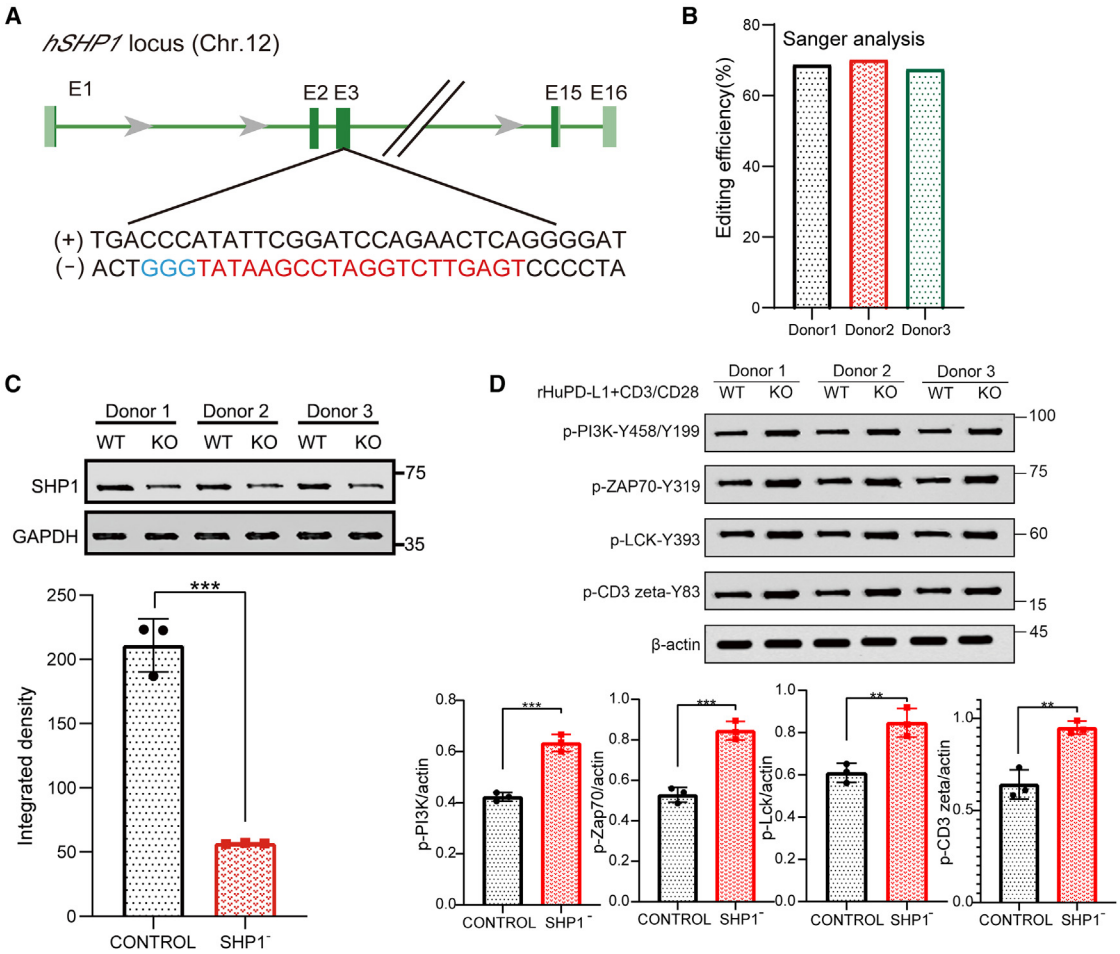

Figure 2. Knockout and post-knockout validation of T cells

(A) Structure of the sgRNA, with the sgRNA sequence and protospacer adjacent motif shown in red and blue, respectively.

(B) Efficiency of the knockout determined using Sanger sequencing.

(C) Western blotting of SHP-1 expression in the knockout and wild-type groups.

(D) Western blotting of the phosphorylation level of the SHP-1 target protein. Each group included three samples (n = 3). $^{**}p < 0.01$, $^{***}p < 0.001$, and $^{****}p < 0.0001$, as assessed using a one-way analysis of variance with Tukey's multiple comparisons post hoc test (C, D). Data are presented as mean ± standard deviation (SD). WB, western blotting.

simvastatin, a lipid metabolism inhibitor, were investigated to enhance their therapeutic efficacy. This research demonstrates the feasibility and efficacy of SHP-1 gene knockout therapy in combination with metabolic inhibitors, advancing adoptive T cell therapy for HCC. The findings could pave the way for new immunotherapeutic strategies that overcome the limitations of the current treatments and provide improved outcomes for HCC patients.

RESULTS

The expression of SHP-1 in exhausted T cells

To investigate the intratumoral T cell SHP-1 expression profile in advanced HCC, single-cell RNA sequencing (scRNA-seq) on tumor biopsy specimens was obtained from 12 patients with advanced HCC and had progressed after targeted therapy and immunotherapy (Figures 1A and S1A). Utilizing the T-distributed stochastic neighbor embedding (t-SNE) method, eight T cell clusters were identified and visualized (Figures 1B, 1C, and S1B). This analysis revealed significantly higher SHP-1 expression in exhausted T cells than in cytotoxic T cells (Figure 1D). Moreover, analysis of two single-cell sequencing datasets from the public GEO database (GSE140228 and GSE98638) revealed that SHP-1 expression was predominantly enriched in $CD8^+$ Tex cells (exhausted $CD8^+$ T cells), with a relatively higher proportion compared to other cell subsets (Figures S1C–S1F).

CRISPR/Cas9 editing system for SHP-1 gene knockout

According to our previous study, an sgRNA with the appropriate knockout effectiveness for the study was selected[10] (Figure 2A). Sanger sequencing showed that the knockout efficiencies of expanded T cells in the three healthy volunteers were 68.7%, 70.1%, and 67.4%, respectively (Figure 2B). Western blotting

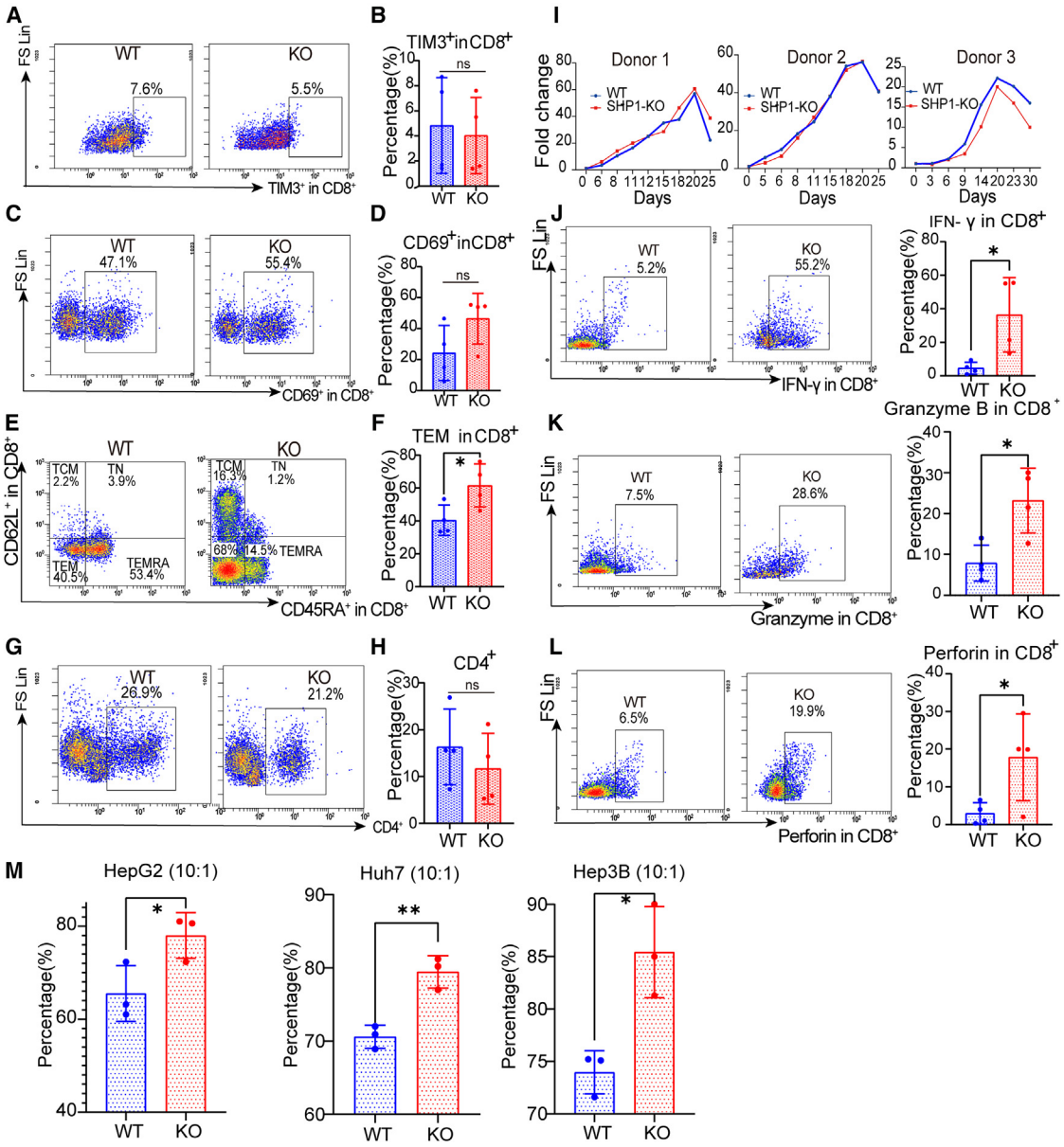

Figure 3. Phenotypic and functional changes of T cell subsets in knockout (KO) and wild-type (WT) groups

(A–F) Expression levels of TIM3 (A, B), CD69 (C, D), and CD62L and CD45RA (E, F) in $CD8^+$ T cells.

(G and H) Changes in $CD4^+$ T cells ($n = 4$ in each group).

(I) T cell proliferation curves from three healthy volunteers.

(J–L) Secretion of IFN-γ (J), Granzyme B (K), and Perforin (L) in KO and WT groups.

(M) Proportion of killed cells when the effector-target ratio of T cells to Hep3B, Huh7, and HepG2 was 10:1. Each group comprised four samples ($n = 4$). $^*p < 0.05$ and $^{**}p < 0.01$, as assessed using a one-way analysis of variance with Tukey's multiple comparisons post hoc test (B, D, F, H) and unpaired Student's t test (J–M). Data are presented as mean ± SD. ns, no significance; KO, knockout; WT, wild type; Sti, stimulation; TCM, central memory T cells; TN, naive T cells; TEM, effector memory T cells; TEMRA, terminal effector memory $CD62L^-CD45RA^+$; SD, standard deviation.

(WB) analysis showed that SHP-1 expression in the KO group was significantly lower than that in the WT group (Figure 2C). The phosphorylation levels of target proteins affected by SHP-1 were detected (Figures 2D and S2). Additionally, SHP-2 expression levels did not differ significantly between the two groups (Figure S3A).

Effect of SHP-1 gene knockout on T cell subsets, proliferation, and cytotoxic function

The proportion of $CD8^+$ T cells in WT and KO groups did not differ significantly (Figure S3B). No significant differences were observed in the expression of PD1, TIM3, or CD69 expression in $CD8^+$ T cells between the groups (Figures 3A–3D and S3C).

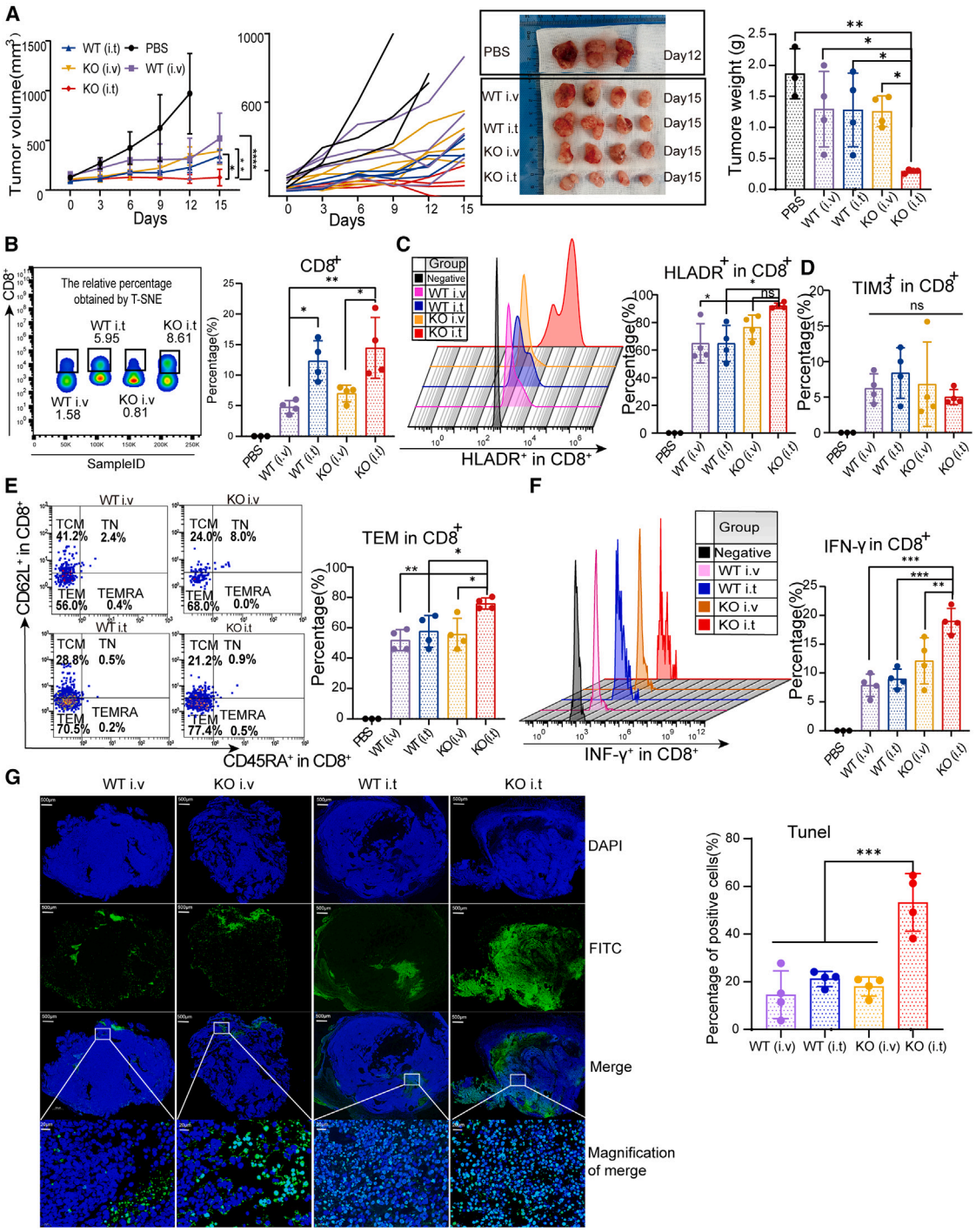

Figure 4. Anti-tumor effect of SHP-1-KO T cells in hepatocellular carcinoma (HCC) patient-derived xenograft (PDX) models

(A) Tumor growth curve, size, and weight after T cell treatment in PDX-5 model, with groups receiving PBS, i.t. injections of WT T cells, and i.v. injections of KO and WT T cells (n = 4 for KO-i.v. and WT-i.v. groups, n = 3 for PBS and WT-i.t. groups).

(B) Relative proportion and quantitative analysis of CD8$^+$ T cells in each group of the PDX-5 model. The relative proportion of CD8$^+$ T cells was obtained by removing bad events in FlowJo using FlowAI, an R plug-in, homogenizing good events through downsampling, and employing t-SNE for dimensionality reduction to display the relative proportion of CD8$^+$ T cells in the four samples.

(C) Proportion and quantitative analysis of HLADR$^+$ expression in CD8$^+$ T cells in each group of the PDX-5 model.

(D) Proportion and quantitative analysis of TIM3$^+$ expression in CD8$^+$ T cells in each group of the PDX-5 model.

(E) Proportion and quantitative analysis of TCM, TN, TEM, and TEMRA in CD8$^+$ T cells of each group in the PDX-5 model.

(legend continued on next page)

The proportion of effector memory T cells (TEM) increased significantly in the KO group than in the WT group (Figures 3E and 3F). No significant differences were observed in the naive T cells (TN), central memory T cells (TCM) between the two groups; however, the proportion of terminally differentiated effector memory $CD45RA^+CD62L^-$ $CD8^+$ T cells (TEMRA) decreased significantly in the KO group. (Figures S3D–S3F). The proportion of $CD4^+$ T cells, regulatory T cells (Tregs), and $CD69^+$ expression in $CD4^+$ T cells were similar in both groups (Figures 3G, 3H, S3G, and S3H). T cell proliferation was not affected by the CRISP/Cas9 editing (Figures 3I, S3I, and S3J). The $CD8^+$ T cells in the KO group secreted higher levels of interferon (IFN)-γ, Granzyme B, and Perforin than in the WT group (Figures 3J–3L). The cytotoxic effect of the KO group was significantly higher in Hep3B, Huh7, and HepG2 cell lines than in the WT group (Figure 3M). The RNA-seq analysis demonstrated that, compared with WT T cells, SHP-1-KO T cells exhibited enhanced anti-tumor functions by improving their adhesion to the extracellular matrix (Figures S4A–S4E).

Anti-tumor effects of SHP-1-KO T cells in HCC PDX models

Twelve tumor samples were collected, and five (41%) were successfully passaged four generations (Figure S5). Hematoxylin and eosin (H&E) staining of the five PDX models showed that tumor cell heterogeneity was preserved (Figure S6). DIR-stained SHP-1-KO T cells were injected intravenously (i.v.) and intratumorally (i.t.) into the PDX-2 model. The i.t. injection resulted a greater cell count than i.v. injection, lasting more than 10 days (Figure S7).

In the PDX-1 preliminary experiment model, the WT group had significantly larger tumor growth rates and weights than the KO group, with no notable differences in body or spleen weights (Figure S8A). Further evaluation in the PDX-3 and PDX-5 models showed that the KO (i.t.) group exhibited slower tumor growth rates and lower tumor weights compared with the WT (i.t.) and WT (i.v.) groups (Figures 4A, S8B, and S8C). The KO (i.t.) group showed higher proportions of $CD8^+$ T cells, $HLADR^+$ expression in $CD8^+$ T cells, and TEM^+CD8^+ T cells, than the other groups (Figures 4B–4E and S8D–S8H). The KO (i.t.) group also showed higher IFN-γ secretion by $CD8^+$ T cells, (Figure 4F), with no significant differences in Granzyme B or Perforin levels (Figures S8I and S8J). TUNEL staining confirmed superior treatment efficacy in the KO (i.t.) group than in the other groups (Figure 4G).

Anti-tumor effects of SHP-1-KO T cells in humanized HCC PDX models

In the PDX-4-1 model, the KO (i.t.) group showed slower tumor growth and lower tumor weight than did the KO (i.v.), WT (i.t.), and WT (i.v.) groups (Figures 5A and 5B). Weight differences in the mouse spleen and body were insignificant (Figure S9A). The proportion of $CD8^+$ T cells in the KO (i.t.) group was larger than those in the KO (i.v.), WT (i.v.), WT (i.t.), and PBS groups (Figure 5C). The proportion of $PD1^+$ and $TIM3^+$ expression in $CD8^+$ T cells in the test groups did not differ significantly (Figures S9B and S9C). The proportion of $HLADR^+$ expression in $CD8^+$ T cells in the KO (i.t.) group was higher than those in the WT (i.t.), WT (i.v.), and PBS groups; Meanwhile, no difference was observed between the KO (i.v.) and KO (i.t.) groups (Figure 5D). The proportion of TEM cells in the KO (i.t.) group was larger than that in the WT (i.t.), WT (i.v.), KO (i.v.), and PBS groups (Figure 5E). The proportion of TEMRA cells in the KO (i.t.) group was lower than that in the WT (i.v.) group, whereas no apparent differences were detected between the KO (i.t.) and KO (i.v.) groups (Figure S9D). The proportion of TCM cells in the KO (i.t.) group was lower than that in the WT (i.t.), WT (i.v.), KO (i.v.), and PBS groups (Figure S9E). Nevertheless, no notable disparities were observed in the proportion of TN cells among the groups (Figure S9F).

The proportion of IFN- γ secreting by $CD8^+$ T cells was considerably higher in the KO (i.t.) group than in the WT (i.t.), WT (i.v.), KO (i.v.) and PBS groups (Figure 5F). Higher levels of $CD8^+$ T cells-secreted Granzyme B was also observed in the KO (i.t.) group than in the WT (i.v.) group; however, no apparent difference was detected in the other three groups (Figure S8G). The level of perforin secreted by $CD8^+$ T cells in the KO (i.t.) group was also higher than that in the WT (i.v.) group; however, no differences were observed between the KO (i.t.) and KO (i.v.) groups (Figure S9H). IHC staining of PDX-4-1 tumors confirmed higher CD8 expression in the KO (i.t.) group than in the WT (i.t.), WT (i.v.), KO (i.v.) and PBS groups (Figure 5G). However, no discernible variations were observed in the proportion of $CD4^+$ T cells or $HLADR^+$ expression in $CD4^+$ T cells or Tregs among the groups (Figures 5H, S9I, and S9J).

In the PDX-4-2 model, the KO (i.t.) group showed significantly slower tumor growth rates and better survival than the other groups (Figures 5I and 5J). No significant differences in body weight were observed across groups (Figure S9K).

Combining SHP-1-KO T cells with simvastatin amplifies the anti-tumor effect

RNA-seq analysis revealed upregulated lipid metabolism pathways in the KO (i.t.) group than the WT (i.t.) group (Figures 6A–6E), while oxidative phosphorylation pathways were downregulated (Figure S10). Additionally, 3-hydroxy-3-methylglutaryl-coenzyme A (HMG-CoA) reductase (*HMGCR*) was identified as a key gene in the lipid metabolism pathway, making it a suitable target for combination therapy (Figure 6F). Public database analysis indicated that *HMGCR* expression levels influenced the overall survival of female patients with

(F) IFN-γ secretion level and quantitative analysis of $CD8^+$ T cells in each group of the PDX-5 model.
(G) Fluorescent TUNEL test and positive cell ratio of paraffin sections of each group in PDX-5 model. $^*p < 0.05$, $^{**}p < 0.01$, $^{***}p < 0.001$, and $^{****}p < 0.0001$, as assessed using a two-way analysis of variance (ANOVA) with Tukey's multiple comparisons post hoc test (A) and one-way ANOVA with Tukey's multiple comparisons post hoc test (A–G). Data are presented as mean ± SD. t-SNE, t-distributed stochastic neighbor embedding; TCM, central memory T cells; TN, naive T cells; TEM, effector memory T cells; TEMRA, terminal effector memory $CD62L^-CD45RA^+$. ns, no significance. i.t., intratumoral injection; i.v., tail vein injection; TUNEL, terminal deoxynucleotidyl transferase dUTP nick end labeling; IFN-γ, interferon-gamma; KO, knock out; WT, wild-type; PBS, phosphate-buffered saline; SHP-1, sarcoma homology 2 domain-containing protein tyrosine phosphatase 1.

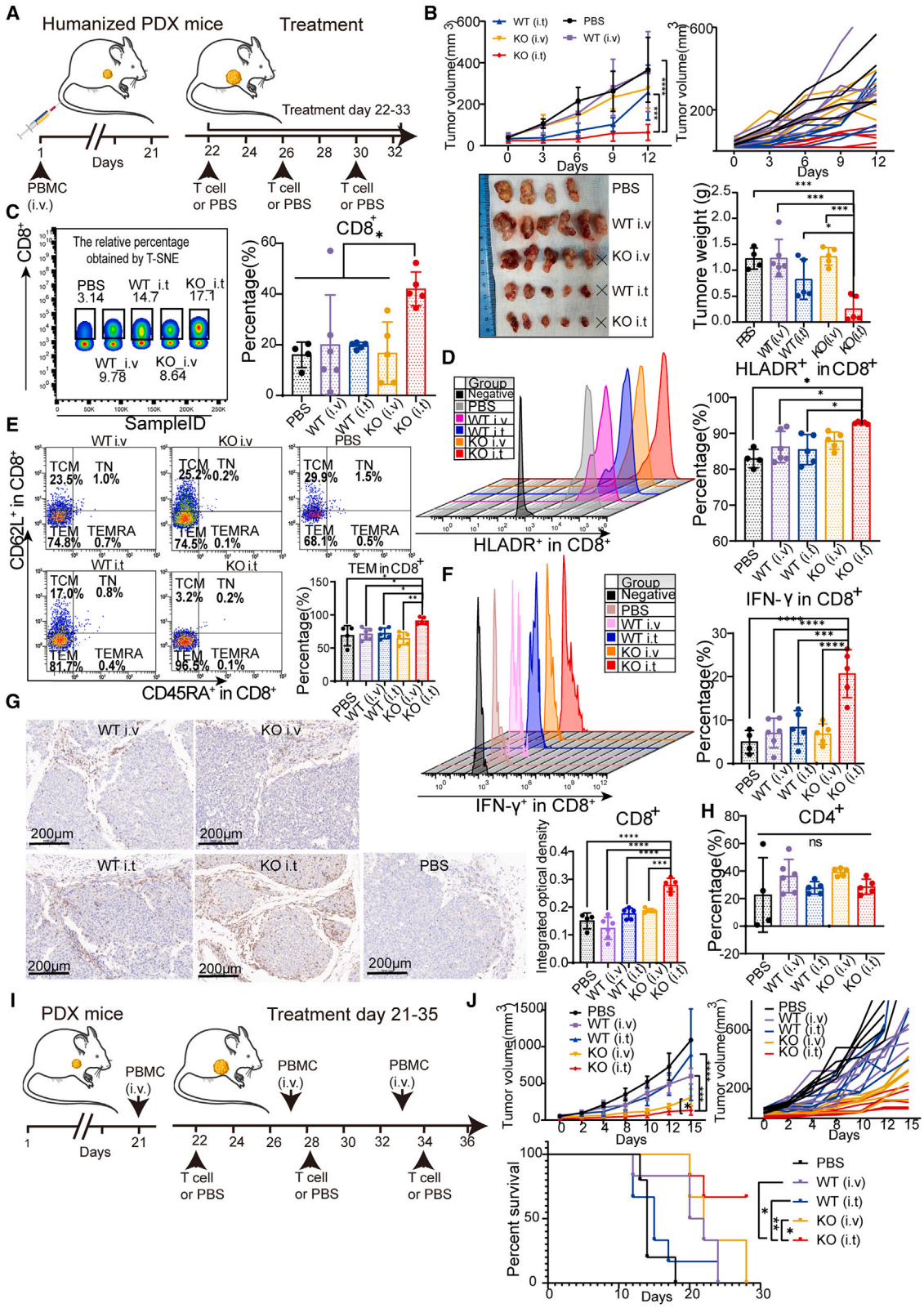

(legend on next page)

HCC (Figures S11A–S11C). Moreover, *in vitro* cytotoxicity assays demonstrated that SHP-1-KO T cells combined with simvastatin exhibited the most potent cytotoxic effect on Huh7 cell line (Figure 7A). In the humanized HCC PDX-4-3 model, combination therapy completely suppressed tumor growth, with superior efficacy compared with the SHP-1-KO T cells or simvastatin monotherapy groups (Figures 7C and S11D). No significant differences in body weight or liver function markers were observed among the treatment groups (Figure 7D).

DISCUSSION

This study demonstrated the feasibility of using CRISPR/Cas9 to knock out SHP-1 in cytotoxic $CD8^+$ T cells, increasing IFN-γ production, extracellular matrix adherence, and anti-tumor activity *in vitro*. In the PDX model, the enhanced anti-tumor effect of SHP-1-KO T cells is attributed to increased TEM cells within the tumor and T cell killing ability, as well as decreased oxidative phosphorylation levels within the tumor. Notably, *in vitro* experiments and the humanized HCC PDX model revealed the combining SHP-1-KO T cells and simvastatin markedly suppresses tumor development.

Statins are FDA-approved HMGCR inhibitors clinically safe and widely used in treating cardiovascular diseases.[13] Moreover, the PDX model is a reliable *in vivo* system that accurately predicts treatment efficacy. Meanwhile, CRISPR/Cas9 editing technology has been proven safe and feasible in a phase I clinical trial by Lu et al.,[14] with edited T cells detectable in peripheral blood for up to four weeks. Therefore, the combinatorial therapy proposed in this study holds significant clinical translational potential. The median of SHP-1 KO efficiency was 68.7% (67.4–70.1%), markedly higher than that of PD1 knockdown in a previous study (16%, 8%–34%).[14] Hence, the CRISPR/Cas9 editing technique is safe and feasible; no discernible variations were observed in the proportion of $CD8^+$ T cells between the KO and WT groups or in the amplification curves of both groups.

In tumor-adoptive cell therapy, long-term preservation of the therapeutic immune cell-killing function depends on the persistence of memory T cells.[15] The *in vitro* analyses in this study revealed that the increased memory cell population in the KO group primarily comprised TEM—a tissue-homing cell with multiple effector functions.[16] In contrast, TCM, which lacks inflammatory response and cytotoxic function yet exhibits lymph node homing,[16,17] showed no difference between the two groups. Additionally, the WT group was more prone to exhaustion because the proportion of TEMRA in the WT group was higher than that in the KO group.[17] Moreover, the KO group secreted more effector cytokines and exhibited a stronger killing capacity in human HCC cell lines than in the WT group. This aligns with the prevailing understanding that TEM cells possess robust cytotoxic capabilities and can generate c myriad efficacious cytokines, including IFN-γ.[17] The enhanced adhesion of the KO group to the extracellular matrix provided a driving force for T cells to the tumor site. Moreover, it facilitated T cell entry into the tumor by adhering to tumor vascular endothelial cells and spreading to the tumor through vascular wall migration.[18,19] Hence, the upregulation of T cell adhesion molecules has the potential to augment the infiltration of anti-tumor T cells, enhancing the effectiveness of adoptive cell therapy.[20]

In PDX and humanized PDX models, SHP-1-KO T cells exhibited anticancer activity, with the KO (i.t.) group demonstrating the highest anti-tumor activity. However, SHP-1 KO in mouse T cells does not impede the development of colon cancer tumors,.[21] as evidenced by the Cre-LoxP method. SHP-1 is critical role in modulating the threshold for positive and negative selection of T cells in the thymus, which is crucial for $CD4^+$ and $CD8^+$ T cell growth and maturation.[5] Hence, the non-selective KO of various T cell subsets, including activated and immature T cells, may have contributed to the lack of an effect. The KO system in the previous study[21] may have disrupted the T cell development and maturation. In contrast, in the current study, the edited T cell population primarily comprised activated $CD8^+$ T cells. Further investigation of the anticancer mechanism of tumor-infiltrating lymphocytes revealed that the proportion of TEM was highest in the KO (i.t.) group, and the secretion of killing factors increased, which was related to the strong cytotoxic function of TEM.[16]

Figure 5. Anti-tumor effect of SHP-1-KO T cells in humanized HCC PDX models

(A) Schematic of the first humanized protocol and treatment scheme for the PDX-4 model (PDX-4-1).

(B) Tumor growth curve, size, and weight after T cell therapy in the humanized PDX-4-1 model (PBS group $n = 4$, KO-i.t. group, KO-i.v. group, WT-i.t. group $n = 5$, and WT-i.v. group $n = 6$).

(C) Relative proportion and quantitative analysis of $CD8^+$ T cells in each group of the humanized PDX-4-1 model. The relative proportion of $CD8^+$ T cells was obtained by removing bad events in FlowJo using FlowAI, an R plug-in, homogenizing good events through downsampling, and employing t-SNE for dimensionality reduction to display the relative proportion of $CD8^+$ T cells in the five samples.

(D) Proportion and quantitative analysis of $HLADR^+$ expression in $CD8^+$ T cells in each group of the humanized PDX-4-1 model.

(E) Proportion and quantitative analysis of TCM, TN, TEM, and TEMRA groups in $CD8^+$ T cells in the humanized PDX-4-1 model.

(F) Secretion level and quantitative analysis of IFN-γ in $CD8^+$ T cells in the humanized PDX-4-1 model.

(G) Immunohistochemical staining of $CD8^+$ T cells in each group of the humanized PDX-4-1 model and the average optical density of each group.

(H) Analysis of the proportion of $CD4^+$ T cells in each group of the humanized PDX-4-1 model.

(I) Schematic of the second humanized protocol for the PDX-4 model (PDX-4-2), PBMC was infused the day before editing T cell infusion (PBS group $n = 5$, KO-i.t., KO-i.v., WT-i.t., and WT-i.v. groups $n = 6$).

(J) Tumor growth curve and survival analysis of each group during the treatment of the humanized PDX-4-2 model. $^*p < 0.05$, $^{**}p < 0.01$, $^{***}p < 0.001$, and $^{****}p < 0.0001$, as assessed using a two-way analysis of variance (ANOVA) with Tukey's multiple comparisons post hoc test (B and J), one-way ANOVA with Tukey's multiple comparisons post hoc test (B–H) and log rank test (J). Data are presented as mean ± SD. t-SNE, t-distributed stochastic neighbor embedding; TCM, central memory T cells; TN, naive T cells; TEM, effector memory T cells; TEMRA, terminal effector memory $CD62L^-CD45RA^+$. ns, no significance. i.t., intratumoral injection; i.v., tail vein injection. × dead; HCC, hepatocellular carcinoma; PDX, patient-derived xenograft; SHP-1, sarcoma homology 2 domain-containing protein tyrosine phosphatase 1; IFN-γ, interferon-gamma; KO, knock out; WT, wild-type; PBS, phosphate-buffered saline; SD, standard deviation.

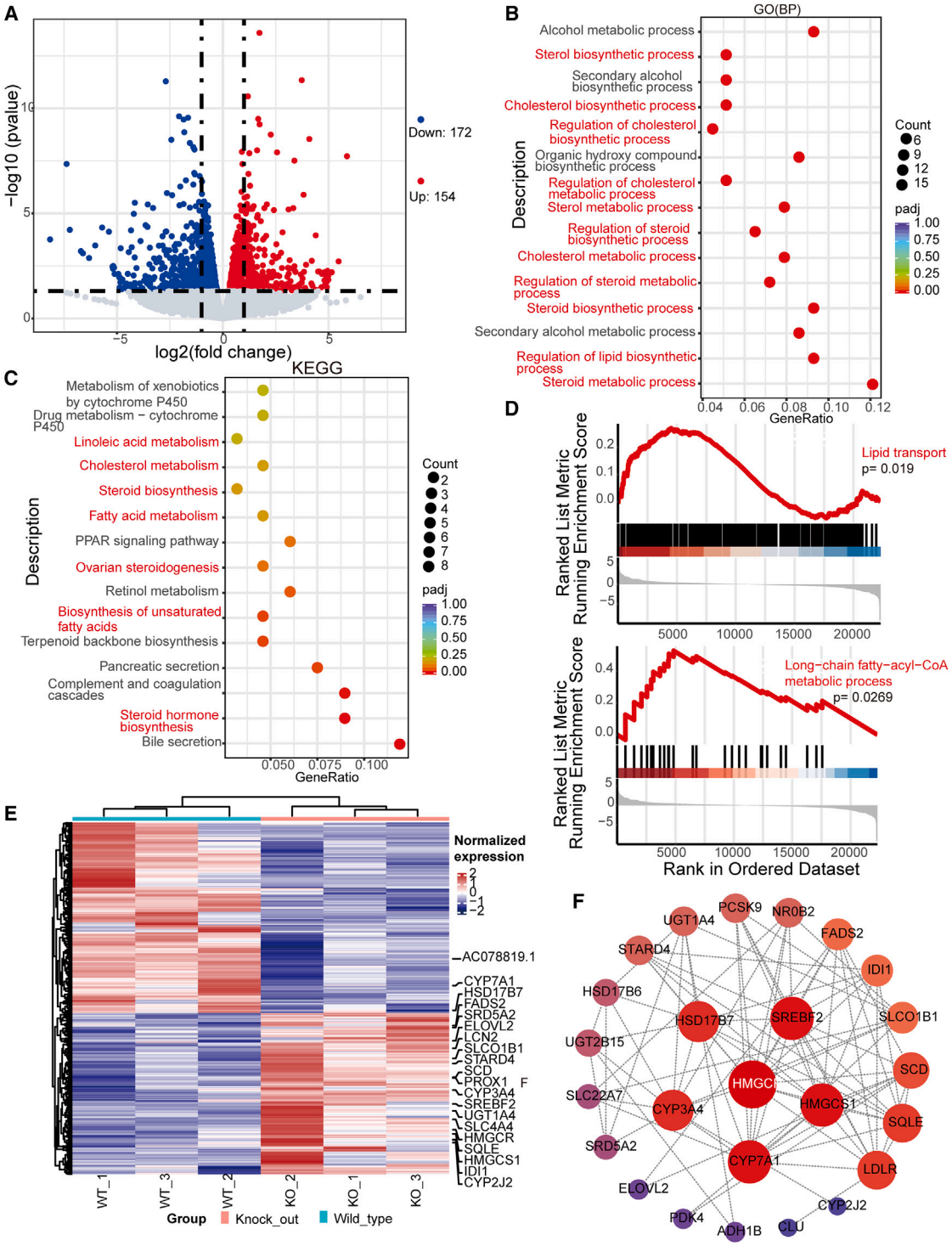

Figure 6. Bulk RNA-seq results of tumor specimens from the KO (i.t.) and WT (i.t.) groups in PDX-3 and PDX-4-1 models

(A) Distribution of up- and down-regulated genes in the PDX-3 model.

(B) Top 15 pathways enriched in GO (BP) analysis of up-regulated genes in the PDX-3 model KO (i.t.) group compared with the WT (i.t.) group.

(C) Top 15 pathways enriched in KEGG analysis of up-regulated genes in the PDX-3 model KO (i.t.) group compared with the WT (i.t.) group.

(D) GSEA analysis of up-regulated genes in the KO (i.t.) group related to the WT (i.t.) group in the PDX-4-1 model.

(E) Expression values of all differential genes in the KO (i.t.) group of the PDX-3 model related to the WT (i.t.) group, with individual labeling of lipid metabolism pathway-related genes.

(legend continued on next page)

The anti-tumor effect of SHP-1-KO T cells may be related to the decreased oxidative phosphorylation of their tumor cells. Drug-resistant tumor areas can be made sensitive to treatment by reducing hypoxia-associated immunosuppression.[22,23] Moreover, contrary to the long-held view that tumors are mostly glycolytic, oxidative phosphorylation active in many malignancies, representing a possible therapeutic target.[24] Therefore, mitochondrial metabolism is important for tumor progression and proliferation.[25] The results of this investigation further substantiated the notion that a diminished level of oxidative phosphorylation within the tumor corresponds to a decelerated proliferation rate. Regarding the mechanism by which SHP-1 KO T cells reduce oxidative phosphorylation levels within the tumor, we hypothesize that this may result from an increased presence of cytotoxic TEM and the secretion of cytotoxic factors, such as IFN-γ, in the KO (i.t.) group than in the controls. This increase in tumor cell killing, as confirmed by TUNEL staining, leads to a reduction in tumor volume. Additionally, tumor proliferation is closely linked to oxidative phosphorylation levels, critical for tumor progression.[25] In the case of B16 melanoma, upregulation of mitochondrial metabolism (oxidative phosphorylation) is pivotal, while the Warburg effect is less relevant.[26] Consequently, in the KO (i.t.) group, the enhanced killing of tumor cells by TEM decreased the number of viable tumor cells, resulting in significantly reduced oxidative phosphorylation levels than that in the controls. However, further investigation is needed to validate this hypothesis.

Here, combining of SHP-1-KO T cells and simvastatin significantly inhibited tumor growth rate *in vitro* and *in vivo*. Simvastatin, a widely used lipid-lowering drug that inhibits HMGCR,[27] augmented the anti-tumor effect of adoptive T cells, suggesting that metabolic reprogramming is a viable approach for reinitiating the immune response against cancer.[28] Dysregulated lipid metabolism, a hallmark of cancer cells, is used to fuel their growth, proliferation, survival, and metastasis, as well as to generate signaling molecules needed for therapy resistance.[29] Therefore, targeting tumor lipid metabolism, such as processes involving fatty acids and cholesterol uptake, key enzymes for lipid synthesis, and lipid oxidation, is a direct strategy for improving the efficacy of immunotherapy.[29,30]

Furthermore, by analyzing the public database, high HMGCR expression was associated with poor prognosis in female patients with HCC, further confirming the potential of targeting tumor lipid metabolism. Although simvastatin inhibits cholesterol synthesis in tumors, whether it also interferes with intratumor T cell activity remains unclear. Previous studies have shown similarities between activated T cells and cancer cells in their metabolic programming,[30,31] suggesting that targeting tumor metabolism also inhibits anti-tumor T cells. However, *in vivo,* this may not always be true, and targeting tumor metabolism may enhance T cell anti-tumor activity.[32,33] Although cancer and T cells share metabolic similarities; cancer cells tend to have more inflexible metabolic processes than T cells, which are more metabolically adaptable.[30] Simvastatin also upregulates cholesterol levels in activated T cells while reducing them in TN,[34] indicating improved effector T cell function. Therefore, simvastatin and SHP-1-KO T cells synergize in killing tumors.

In conclusion, this study demonstrated that SHP-1-KO T cells generated using CRISPR/Cas9 technology exhibit enhanced anti-tumor effects *in vitro* and in HCC PDX models. Combining these edited T cells with simvastatin significantly improves their therapeutic efficacy, providing a promising strategy for developing more effective HCC treatments.

Limitations of the study

This study has certain limitations. First, the T cell adhesion function of SHP-1 KO was not validated functionally. Second, subcutaneous models were used in PDX models instead of orthotopic models due to the difficulty in constructing orthotopic PDX models of HCC. Third, PBMCs were injected into the tail vein for immune system reconstitution in PDX models instead of using hematopoietic stem cell transplantation, which has a low success rate and is difficult to acquire. In addition, the present study lacks the assessment of serum markers of HCC, such as alpha-fetoprotein, due to limited serum availability in the experimental design.

RESOURCE AVAILABILITY

Lead contact

Requests for resources, reagents, and further information should be directed to the lead contact, Wei Wang (wang_w@csu.edu.cn).

Materials availability

All mouse lines and materials used in this study were provided or purchased from mentioned companies or researchers. This study did not generate any new or unique reagents.

Data and code availability

- RNA-seq data have been deposited at SRA and are publicly available as of the date of publication. Accession numbers are listed in the key resources table.
- This article does not report the original code.
- Any additional information required to reanalyze the data reported in this article is available from the lead contact upon request.

ACKNOWLEDGMENTS

We sincerely thank our relatives (Silian Luo, Touying Liu, Zhaoqi Liu, etc.) for taking care of the family and allowing us to have the time and energy to do this study. This project was supported by grants from the National Natural Science Foundation of China (Grant No: 82372071 and 82272102) and the Key Project of the Science and Technology Program of Hunan Province (Grant No.2023ZJ1100) Graphical abstract was created with BioRender.com.

AUTHOR CONTRIBUTIONS

H.L., X.M., and W.W. designed the experiments. H.L. wrote the manuscript. W.L., X.M., and W.W. revised the article. H.L., W.G., X.Y., J.L., J.Z., M.Y.,

(F) Protein–protein interaction (PPI) networks plots of the top 25 lipid metabolism pathway-related genes in the PDX-3 model, with larger circles and redder colors indicating higher weights. $n = 3$/groups; red marker pathway: related to lipid metabolism. PPI, Protein–protein Interaction Networks. i.t., intratumoral injection; i.v., tail vein injection; GO, Gene Ontology; KEGG, Kyoto Encyclopedia of Genes and Genomes; BP, biological process; GSEA, Gene Set Enrichment Analysis.

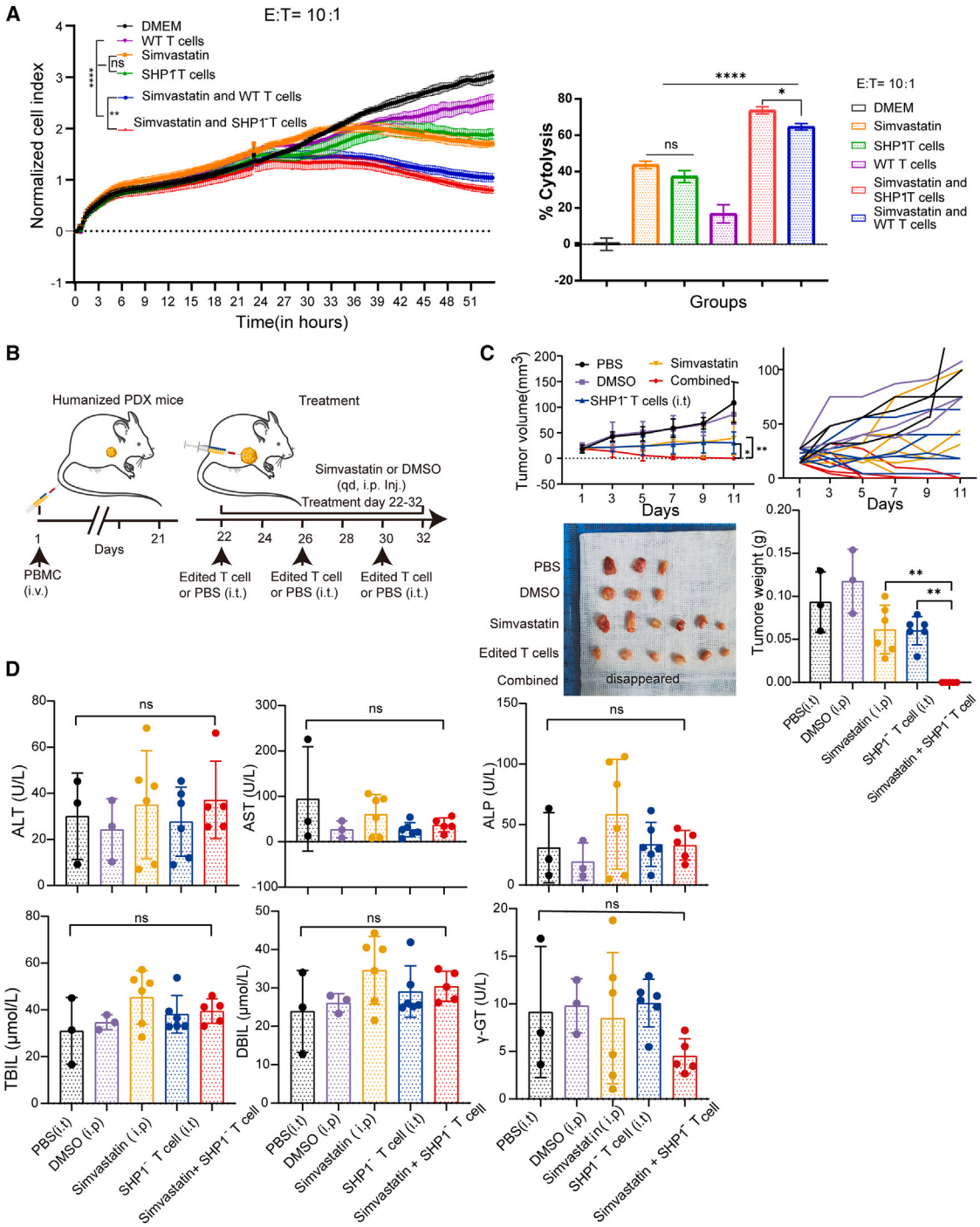

Figure 7. Combining edited T cells with simvastatin exerts significant anti-tumor effects in the HCC PDX model

(A) Cytotoxicity assay of T cells in combined with simvastatin.

(B) Humanization protocol and treatment regimen for the PDX-4-3 model.

(C) Tumor growth curves, tumor specimen sizes, and tumor weights changes during treatment in each group at the experimental cutoff point. (PBS group $n = 3$, DMSO group $n = 3$, simvastatin group $n = 6$, edited T cell group $n = 6$, and combination drug group $n = 6$).

(D) Liver function indexes, including ALT, AST, TBIL, DBIL, ALP, and γ-GT, were measured in all groups of mice. $^{*}p < 0.05$, $^{**}p < 0.01$, as assessed using a two-way analysis of variance (ANOVA) with Tukey's multiple comparisons post hoc test (A, C) and one-way ANOVA with Tukey's multiple comparisons post hoc test (C, D). Data are presented as mean ± SD. ALT, Alanine aminotransferase; AST, Aspartate aminotransferase; TBIL, Total bilirubin; DBIL, Direct Bilirubin; ALP, Alkaline phosphatase; γ-GT, γ- Gamma-glutamyl transpeptidase. ns, no significance. i.t., intratumoral injection; i.v., tail vein injection; i.p, intraperitoneal injection.; HCC, hepatocellular carcinoma; PDX, patient-derived xenograft; HMGCR, 3-hydroxy-3-methylglutaryl-coenzyme A (CoA) reductase.

L.C., Y.Z., R.W., C.Y., P.L., M.T., P.P., L.P., D.W., M.L., Q.L., S.Z., W.L., P.R., and H.L. performed the experiments and analyzed the data. X.M. and W.W. are responsible for the overall content as guarantors. All authors read and approved the final manuscript.

DECLARATION OF INTERESTS

The authors declare no competing interests.

STAR★METHODS

Detailed methods are provided in the online version of this paper and include the following:

- KEY RESOURCES TABLE
- EXPERIMENTAL MODEL AND STUDY PARTICIPANT DETAILS
  - Ethics statement
  - Tumour cell lines
  - Mice
- METHOD DETAILS
  - Single-cell sequencing
  - CRISPR/Cas9-mediated SHP-1 gene knockout
  - Western blotting
  - Cell cultures and cytotoxicity assay
  - DIR staining method for T cells
  - Cytotoxicity assay of T cells combined with simvastatin
  - Flow cytometry
  - HCC PDX models, H&E staining, TUNEL assay, and IHC staining
  - Whole transcriptome sequencing
- QUANTIFICATION AND STATISTICAL ANALYSIS

SUPPLEMENTAL INFORMATION

Supplemental information can be found online at https://doi.org/10.1016/j.isci.2025.112266.

Received: August 7, 2024
Revised: December 4, 2024
Accepted: March 18, 2025
Published: March 22, 2025

REFERENCES

1. Llovet, J.M., Kelley, R.K., Villanueva, A., Singal, A.G., Pikarsky, E., Roayaie, S., Lencioni, R., Koike, K., Zucman-Rossi, J., and Finn, R.S. (2021). Hepatocellular carcinoma. Nat. Rev. Dis. Primers *7*, 6. https://doi.org/10.1038/s41572-020-00240-3.
2. Llovet, J.M., Zucman-Rossi, J., Pikarsky, E., Sangro, B., Schwartz, M., Sherman, M., and Gores, G. (2016). Hepatocellular carcinoma. Nat. Rev. Dis. Primers *2*, 16018. https://doi.org/10.1038/nrdp.2016.18.
3. Villanueva, A. (2019). Hepatocellular Carcinoma. N. Engl. J. Med. *380*, 1450–1462. https://doi.org/10.1056/NEJMra1713263.
4. Wolchok, J.D., Neyns, B., Linette, G., Negrier, S., Lutzky, J., Thomas, L., Waterfield, W., Schadendorf, D., Smylie, M., Guthrie, T., Jr., et al. (2010). Ipilimumab monotherapy in patients with pretreated advanced melanoma: a randomised, double-blind, multicentre, phase 2, dose-ranging study. Lancet Oncol. *11*, 155–164. https://doi.org/10.1016/S1470-2045(09)70334-1.
5. Lorenz, U. (2009). SHP-1 and SHP-2 in T cells: two phosphatases functioning at many levels. Immunol. Rev. *228*, 342–359. https://doi.org/10.1111/j.1600-065X.2008.00760.x.
6. Kilgore, N.E., Carter, J.D., Lorenz, U., and Evavold, B.D. (2003). Cutting edge: dependence of TCR antagonism on Src homology 2 domain-containing protein tyrosine phosphatase activity. J. Immunol. *170*, 4891–4895. https://doi.org/10.4049/jimmunol.170.10.4891.
7. Sathish, J.G., Dolton, G., Leroy, F.G., and Matthews, R.J. (2007). Loss of Src homology region 2 domain-containing protein tyrosine phosphatase-1 increases CD8+ T cell-APC conjugate formation and is associated with enhanced *in vivo* CTL function. J. Immunol. *178*, 330–337. https://doi.org/10.4049/jimmunol.178.1.330.
8. Sathish, J.G., Johnson, K.G., LeRoy, F.G., Fuller, K.J., Hallett, M.B., Brennan, P., Borysiewicz, L.K., Sims, M.J., and Matthews, R.J. (2001). Requirement for CD28 co-stimulation is lower in SHP-1-deficient T cells. Eur. J. Immunol. *31*, 3649–3658. https://doi.org/10.1002/1521-4141(200112)31:12<3649::aid-immu3649>3.0.co;2-8.
9. Snook, J.P., Soedel, A.J., Ekiz, H.A., O'Connell, R.M., and Williams, M.A. (2020). Inhibition of SHP-1 Expands the Repertoire of Antitumor T Cells Available to Respond to Immune Checkpoint Blockade. Cancer Immunol. Res. *8*, 506–517. https://doi.org/10.1158/2326-6066.cir-19-0690.
10. Liu, M., Zhang, L., Zhong, M., Long, Y., Yang, W., Liu, T., Huang, X., and Ma, X. (2023). CRISPR/Cas9-mediated knockout of intracellular molecule SHP-1 enhances tumor-killing ability of CD133-targeted CAR T cells *in vitro*. Exp. Hematol. Oncol. *12*, 88. https://doi.org/10.1186/s40164-023-00450-x.
11. Yi, T., Elson, P., Mitsuhashi, M., Jacobs, B., Hollovary, E., Budd, G.T., Spiro, T., Triozzi, P., and Borden, E.C. (2011). Phosphatase inhibitor, sodium stibogluconate, in combination with interferon (IFN) alpha 2b: phase I trials to identify pharmacodynamic and clinical effects. Oncotarget *2*, 1155–1164. https://doi.org/10.18632/oncotarget.393.
12. Dempke, W.C.M., Uciechowski, P., Fenchel, K., and Chevassut, T. (2018). Targeting SHP-1, 2 and SHIP Pathways: A Novel Strategy for Cancer Treatment? Oncology *95*, 257–269. https://doi.org/10.1159/000490106.
13. Gidding, S.S., Champagne, M.A., de Ferranti, S.D., Defesche, J., Ito, M.K., Knowles, J.W., McCrindle, B., Raal, F., Rader, D., Santos, R.D., et al. (2015). The Agenda for Familial Hypercholesterolemia: A Scientific Statement From the American Heart Association. Circulation *132*, 2167–2192. https://doi.org/10.1161/CIR.0000000000000297.
14. Lu, Y., Xue, J., Deng, T., Zhou, X., Yu, K., Deng, L., Huang, M., Yi, X., Liang, M., Wang, Y., et al. (2020). Safety and feasibility of CRISPR-edited T cells in patients with refractory non-small-cell lung cancer. Nat. Med. *26*, 732–740. https://doi.org/10.1038/s41591-020-0840-5.
15. Busch, D.H., Fräßle, S.P., Sommermeyer, D., Buchholz, V.R., and Riddell, S.R. (2016). Role of memory T cell subsets for adoptive immunotherapy. Semin. Immunol. *28*, 28–34. https://doi.org/10.1016/j.smim.2016.02.001.
16. Sallusto, F., Lenig, D., Förster, R., Lipp, M., and Lanzavecchia, A. (1999). Two subsets of memory T lymphocytes with distinct homing potentials and effector functions. Nature *401*, 708–712. https://doi.org/10.1038/44385.
17. Mueller, S.N., Gebhardt, T., Carbone, F.R., and Heath, W.R. (2013). Memory T cell subsets, migration patterns, and tissue residence. Annu. Rev. Immunol. *31*, 137–161. https://doi.org/10.1146/annurev-immunol-032712-095954.
18. Liu, Y.-T., and Sun, Z.-J. (2021). Turning cold tumors into hot tumors by improving T-cell infiltration. Theranostics *11*, 5365–5386. https://doi.org/10.7150/thno.58390.
19. Fierro Morales, J.C., Xue, Q., and Roh-Johnson, M. (2022). An evolutionary and physiological perspective on cell-substrate adhesion machinery for cell migration. Front. Cell Dev. Biol. *10*, 943606. https://doi.org/10.3389/fcell.2022.943606.
20. Wang-Bishop, L., Kimmel, B.R., Ngwa, V.M., Madden, M.Z., Baljon, J.J., Florian, D.C., Hanna, A., Pastora, L.E., Sheehy, T.L., Kwiatkowski, A.J., et al. (2023). STING-activating nanoparticles normalize the vascular-immune interface to potentiate cancer immunotherapy. Sci. Immunol. *8*, eadd1153. https://doi.org/10.1126/sciimmunol.add1153.
21. Ventura, P.M.O., Gakovic, M., Fischer, B.A., Spinelli, L., Rota, G., Pathak, S., Khameneh, H.J., Zenobi, A., Thomson, S., Birchmeier, W., et al. (2022). Concomitant deletion of Ptpn6 and Ptpn11 in T cells fails to improve anticancer responses. EMBO Rep. *23*, e55399. https://doi.org/10.15252/embr.202255399.

22. De Bruycker, S., Vangestel, C., Van den Wyngaert, T., Pauwels, P., Wyffels, L., Staelens, S., and Stroobants, S. (2019). (18)F-Flortanidazole Hypoxia PET Holds Promise as a Prognostic and Predictive Imaging Biomarker in a Lung Cancer Xenograft Model Treated with Metformin and Radiotherapy. J. Nucl. Med. *60*, 34–40. https://doi.org/10.2967/jnumed.118.212225.

23. Scharping, N.E., Menk, A.V., Whetstone, R.D., Zeng, X., and Delgoffe, G.M. (2017). Efficacy of PD-1 Blockade Is Potentiated by Metformin-Induced Reduction of Tumor Hypoxia. Cancer Immunol. Res. *5*, 9–16. https://doi.org/10.1158/2326-6066.CIR-16-0103.

24. Vasan, K., Werner, M., and Chandel, N.S. (2020). Mitochondrial Metabolism as a Target for Cancer Therapy. Cell Metab. *32*, 341–352. https://doi.org/10.1016/j.cmet.2020.06.019.

25. Faubert, B., Solmonson, A., and DeBerardinis, R.J. (2020). Metabolic reprogramming and cancer progression. Science *368*, eaaw5473. https://doi.org/10.1126/science.aaw5473.

26. Zdralevic, M., Brand, A., Di Ianni, L., Dettmer, K., Reinders, J., Singer, K., Peter, K., Schnell, A., Bruss, C., Decking, S.M., et al. (2018). Double genetic disruption of lactate dehydrogenases A and B is required to ablate the "Warburg effect" restricting tumor growth to oxidative metabolism. J. Biol. Chem. *293*, 15947–15961. https://doi.org/10.1074/jbc.RA118.004180.

27. Hamelin, B.A., and Turgeon, J. (1998). Hydrophilicity/lipophilicity: relevance for the pharmacology and clinical effects of HMG-CoA reductase inhibitors. Trends Pharmacol. Sci. *19*, 26–37. https://doi.org/10.1016/s0165-6147(97)01147-4.

28. Chen, D., Barsoumian, H.B., Fischer, G., Yang, L., Verma, V., Younes, A.I., Hu, Y., Masropour, F., Klein, K., Vellano, C., et al. (2020). Combination treatment with radiotherapy and a novel oxidative phosphorylation inhibitor overcomes PD-1 resistance and enhances antitumor immunity. J. Immunother. Cancer *8*, e000289. https://doi.org/10.1136/jitc-2019-000289.

29. Bian, X., Liu, R., Meng, Y., Xing, D., Xu, D., and Lu, Z. (2021). Lipid metabolism and cancer. J. Exp. Med. *218*, e20201606. https://doi.org/10.1084/jem.20201606.

30. Leone, R.D., and Powell, J.D. (2021). Fueling the Revolution: Targeting Metabolism to Enhance Immunotherapy. Cancer Immunol. Res. *9*, 255–260. https://doi.org/10.1158/2326-6066.CIR-20-0791.

31. Wang, R., Dillon, C.P., Shi, L.Z., Milasta, S., Carter, R., Finkelstein, D., McCormick, L.L., Fitzgerald, P., Chi, H., Munger, J., and Green, D.R. (2011). The transcription factor Myc controls metabolic reprogramming upon T lymphocyte activation. Immunity *35*, 871–882. https://doi.org/10.1016/j.immuni.2011.09.021.

32. Leone, R.D., Zhao, L., Englert, J.M., Sun, I.M., Oh, M.H., Sun, I.H., Arwood, M.L., Bettencourt, I.A., Patel, C.H., Wen, J., et al. (2019). Glutamine blockade induces divergent metabolic programs to overcome tumor immune evasion. Science *366*, 1013–1021. https://doi.org/10.1126/science.aav2588.

33. Kansal, V., Burnham, A.J., Kinney, B.L.C., Saba, N.F., Paulos, C., Lesinski, G.B., Buchwald, Z.S., and Schmitt, N.C. (2023). Statin drugs enhance responses to immune checkpoint blockade in head and neck cancer models. J. Immunother. Cancer *11*, e005940. https://doi.org/10.1136/jitc-2022-005940.

34. Zhang, Y., Vu, T., Palmer, D.C., Kishton, R.J., Gong, L., Huang, J., Nguyen, T., Chen, Z., Smith, C., Livák, F., et al. (2022). A T cell resilience model associated with response to immunotherapy in multiple tumor types. Nat. Med. *28*, 1421–1431. https://doi.org/10.1038/s41591-022-01799-y.

35. Kong, Y., Sheng, X., Wu, X., Yan, J., Ma, M., Yu, J., Si, L., Chi, Z., Cui, C., Dai, J., et al. (2017). Frequent Genetic Aberrations in the CDK4 Pathway in Acral Melanoma Indicate the Potential for CDK4/6 Inhibitors in Targeted Therapy. Clin. Cancer Res. *23*, 6946–6957. https://doi.org/10.1158/1078-0432.CCR-17-0070.

36. Zheng, X., Yan, J., You, W., Li, F., Diao, J., He, W., and Yao, Y. (2021). De Novo Nano-Erythrocyte Structurally Braced by Biomimetic Au(I)-peptide Skeleton for MDM2/MDMX Predation toward Augmented Pulmonary Adenocarcinoma Immunotherapy. Small *17*, e2100394. https://doi.org/10.1002/smll.202100394.

37. Hu, Z., Zheng, X., Jiao, D., Zhou, Y., Sun, R., Wang, B., Tian, Z., and Wei, H. (2020). LunX-CAR T Cells as a Targeted Therapy for Non-Small Cell Lung Cancer. Mol. Ther. Oncolytics *17*, 361–370. https://doi.org/10.1016/j.omto.2020.04.008.

STAR★METHODS

KEY RESOURCES TABLE

REAGENT or RESOURCE	SOURCE	IDENTIFIER
Antibodies		
Anti-human SHP-1	Abcam	Cat# ab131537
Anti-human p-CD3 zeta-Y83	Abcam	Cat# ab68236
Anti-human CD3 zeta	Abcam	Cat#ab243874
Anti-human p-PI3K-Y458/Y199	Abcam	Cat# ab278545
Anti-human PI3K	Abcam	Cat# ab283852
Anti-human p-ZAP70-Y319	Abcam	Cat# ab194792
Anti-human ZAP70	Abcam	Cat#ab302821
Anti-human p-LCK-Y393	Abcam	Cat# ab138442
Anti-human LCK	Abcam	Cat# ab227975
Anti-human GAPDH	Abcam	Cat# ab8245
Anti-human Actin	Abcam	Cat# ab8266
Anti-human CD45-FITC	BD Biosciences	Cat# 347463
Anti-human CD8-FITC	BD Biosciences	Cat# 551347
Anti-human TIM3-PE	BD Biosciences	Cat# 563422
Anti-human CD45-PE Cy5	BD Biosciences	Cat# 552888
Anti-human PD1- PE Cy7	BD Biosciences	Cat# 561272
Anti-human HLA-DR- FITC	BD Biosciences	Cat# 555560
Anti-human CD4-PE	BD Biosciences	Cat# 555347
Anti-human CD8-PE Cy5	BD Biosciences	Cat# 555368
Anti-human CD69- PE Cy7	BD Biosciences	Cat# 560712
Anti-human CD62L-PE	BD Biosciences	Cat# 555544
Anti-human CD45RA- PE Cy5	BD Biosciences	Cat# 555490
Anti-human CD45-PE Cy7	BD Biosciences	Cat# 557748
Anti-human CD4- FITC	BD Biosciences	Cat# 555346
Anti-human CD127- PE	BD Biosciences	Cat# 557938
Anti-human CD25- PE Cy5	BD Biosciences	Cat# 555433
Anti-human IFN-γ- PE	BD Biosciences	Cat# 559327
Anti-human Granzyme B- PE	BD Biosciences	Cat# 561142
Anti-human Perforin- PE	BD Biosciences	Cat# 563763
Anti-human Fc-blocked	BD Biosciences	Cat# 564220
Anti- CD8 alpha Rabbit pAb	Wuhan Servicebio Technology Co., Ltd (Wuhan China)	#GB114123-100
Chemicals, peptides, and recombinant proteins		
CTS Immune Cell Serum Replacement	Gibco	Cat# A2596101
Propidium iodide	BD Biosciences	Cat# 556547
Cytofix/Cytoperm™ fixation and permeabilisation solution	BD Biosciences	Cat# 554714
Simvastatin	Selleck, USA	Cat# MK733
Deposited data		
Transcriptome sequencing	This article; Mendeley Data	https://doi.org/10.17632/gnkgbjpc2x.1 https://doi.org/10.17632/gnkgbjpc2x.1
scRNAseq raw data	GEO database (https://www.ncbi.nlm.nih.gov/geo/)	GSE140228 and GSE98638

(*Continued on next page*)

Continued

REAGENT or RESOURCE	SOURCE	IDENTIFIER
scRNAseq raw data	This article (https://www.ncbi.nlm.nih.gov/geo/)	GSE290925
Experimental models: Cell lines		
Hep3B	Wuhan Pricella Biotechnology Co., Ltd (Wuhan, Hubei, China)	Cat# CL-0102
HepG2	Wuhan Pricella Biotechnology Co., Ltd (Wuhan, Hubei, China)	Cat# CL-0103
Huh7	Wuhan Pricella Biotechnology Co., Ltd (Wuhan, Hubei, China)	Cat# CL-0120
Experimental models: Organisms/strains		
NOD/ShiLtJGpt-Prkdcem26Cd52Il2rgem26Cd22/Gpt (NCG) mice	GemPharmatech Co., Ltd (Nanjing, China)	Strain NO. T001475
Oligonucleotides		
Primer sequences for qPCR	Table S1	N/A
Software and algorithms		
R version 4.2.3	R Development Core Team	https://www.r-project.org
GraphPad Prism version 9.0	GraphPad Software	https://www.graphpad.com
FlowJov.10.5.3	Treestar	https://www.flowjo.com/solutions/flowjo/downloads
Illustrator	Adobe	https://www.adobe.com
Image J	NIH	https://imagej.nih.gov
Cytoscape	Cytoscape	https://cytoscape.org/
Other		
Anti-CD3/anti-CD28 Dynabeads	Gibco	Cat# 11161D
Nucleofector 4D	Lonza	Cat# AAF-1003X
P3 Primary Cell Solution Box Kit (PBP3)-02250	Lonza	Cat# V4XP-3032
CFSE[5-(and 6)-Carboxyfluorescein diacetate,succinimidyl ester]	AAT Bioquest, USA	Cat# 22022
Cytomics FC 500 flow cytometer	BECKMAN COULTER	NA

EXPERIMENTAL MODEL AND STUDY PARTICIPANT DETAILS

Ethics statement

This study was conducted under the Declaration of Helsinki and was approved by the Third Xiangya Hospital Ethics Committee of Central South University (Ethics number: R19021). All patients provided written informed consent.

Tumour cell lines

Human HCC cell lines HepG2 (#CL-0103), Huh7 (#CL-0120), and Hep3B (#CL-0102) were obtained from Wuhan Procell Life Science & Technology Co., Ltd. and cultured in Dulbecco's Modified Eagle Medium (DMEM) with 1% streptomycin and penicillin and 10% FBS.

Mice

NOD/ShiLtJGpt-Prkdcem26Cd52Il2rgem26Cd22/Gpt (NCG) mice (Strain NO. T001475) were obtained from GemPharmatech (Nanjing, China) and housed in a pathogen-free environment. Unless otherwise noted, 8-week-old male mice were used for all experiments.

METHOD DETAILS

Single-cell sequencing

Tumour biopsy specimens from advanced hepatocellular carcinoma (HCC) patients who had progressed following targeted therapy and immunotherapy were submitted to OE Biotech Co., Ltd. (Shanghai, China) for single-cell RNA sequencing (scRNA-seq) analysis.

Briefly, fresh biopsies were digested in DMEM/F12 with Liberase TL (Roche, USA) and 200 U mL/DNase I (Thermo Fisher Scientific, USA), then filtered and resuspended in RPMI-1640. Single-cell gel beads in emulsions (GEMs) were created using the Chromium Single-Cell Controller (10× Genomics), generating barcoded cDNA, amplified and sequenced on a NovaSeq 6000 (Illumina, USA). Cell Ranger software (version 3.1.0) facilitated demultiplexing and mapping, with quality control and integration using Seurat (Version 3.1.2), filtering for cell viability and mitochondrial gene expression. Differentially expressed genes (DEGs) were identified with the FindAllMarkers function (test.use = bimod). The aim was to examine the intratumoural T cell SHP-1 expression profile in advanced HCC. In addition, we analyzed the expression of SHP-1 in T cell subsets in HCC samples using GEO database (https://www.ncbi.nlm.nih.gov/).

CRISPR/Cas9-mediated SHP-1 gene knockout

Peripheral venous blood was collected from healthy individuals who volunteered and provided written informed consent. The peripheral blood samples (20 mL) were separated using centrifugation on a Ficoll density gradient. T cells were stimulated with anti-CD3/anti-CD28 Dynabeads (Gibco, USA) for 3–5 days at 37°C in a 5% CO_2 incubator, single guide (sg)RNA was used to delete SHP-1 by targeting exon 3 (Figure 1A). Cas9: sgRNA ribonucleoproteins were co-transfected into activated T cells using Nucleofector 4D (Lonza, Germany) and the P3 Primary Cell Solution Box Kit (PBP3)-02250 (Lonza, Germany). An AIM-V medium with 300 U/mL of interleukin-2 (IL-2) and CTS Immune Cell Serum Replacement (Gibco, USA) was used to expand the cells after electroporation for 20–28 days. The medium was replaced every 2–3 days, yielding approximately 2×10^8 cells per volunteer, with > 90% cell viability at the end of the expansion period (21 days). Editing efficiency was assessed using PCR-Sanger sequencing 7–14 days post-electroporation, and gene deletions were validated using western blotting (WB). During T-cell expansion, WT and KO T cells were counted every 2–3 days. Viable cells were stained with AO/PI dye (Biogradetech, USA) and analysed using an automated cell counter (RWD, China). The total number of viable cells was recorded, and T-cell expansion curves were generated. Additionally, CFSE (AAT Bioquest, USA) staining was performed on KO and WT T cells, followed by stimulation with anti-CD3/anti-CD28 Dynabeads (Gibco, USA) for 4 days. T-cell proliferation activity was then analysed using a BD Biosciences flow cytometer (San Diego, CA, USA). This assay enabled a comparative analysis of proliferation between the two groups.

Western blotting

SHP-1 protein levels in KO and WT groups were evaluated by WB to confirm successful SHP-1 elimination. After 8 h of stimulation with human recombinant PD-L1 protein, the phosphorylation levels of the target proteins interacting with SHP-1 in T cells were assessed. Primary antibodies used included rabbit anti-human SHP-1(Abcam, UK), CD3-Y83 (Abcam, UK), p-PI3K-Y458/Y199, PI3K (Abcam, UK), p-ZAP70-Y319, ZAP70 (Abcam, UK), and p-LCK-Y393, LCK (Abcam, UK). Mouse anti-human GAPDH (Abcam, UK) or -actin (Abcam, UK) served as internal control.

Cell cultures and cytotoxicity assay

SHP-1-KO and WT T cells were cultured in RPMI-1640 medium supplemented with IL-2 (400 IU/mL) and 10% foetal bovine serum (FBS). Human HCC, HepG2, Huh7, and Hep3B cells were obtained from Wuhan Procell Life Science & Technology Co., Ltd. and cultured in DMEM with 1% streptomycin and penicillin and 10% FBS.

Cytotoxicity of T cells was assessed using flow cytometry. Co-cultures of HepG2, Huh7, Hep3B, and expanded T cells at a 1:10 ratio were incubated for 8 h. Samples were stained with CD45 antibody (FITC mouse anti-human; BD Biosciences) and propidium iodide (PI; Annexin V Apoptosis Detection Kit I, BD Biosciences) and analysed using the Cytomics FC 500 flow cytometer (Beckman Coulter, USA). The percentage of eliminated tumour cells was determined using the $CD45^-PI^+$ population. Specific methods for the cytotoxicity assay of T cells in combination with simvastatin are provided in the supplemental information.

DIR staining method for T cells

SHP-1-KO T cells and WT T cells were incubated with 2.5 μg/mL DiR (#D12731, ThermoFisher) staining solution for 5 min, washed twice with homemade termination solution (1640 medium +10% FBS), and resuspended in normal saline and injected into mice.

Cytotoxicity assay of T cells combined with simvastatin

T cell-mediated lysis of Huh7 cells was assessed by RTCA, a label-free, real-time monitoring assay of adherent cell lysis by measuring impedance. Briefly, Huh7 adherent targets (5,000 cells) were seeded into the wells of E-Plates 16 PET (#300600890, Agilent, China) in 100 μL of media; their adhesion was monitored for 24 h. T cells were added in 100 μL/well. Co-cultures were assessed by the system with a measure of cell index every 15 min for up to 54 h. The SHP-1-KO or WT T cells were co-cultured at a 10:1 E/T ratio. The administration concentration of simvastatin (#MK733; Selleck, USA) was 30 μM. The results of cytotoxicity were expressed as cell index.

Flow cytometry

Phenotypic analysis of expanded T cells (SHP-1-KO and WT groups) was performed using antibodies from BD Biosciences (San Diego, CA, USA): FITC CD8, PE TIM3, PE-Cy5 CD45, PE-Cy7 PD1, FITC HLA-DR, PE CD4, PE-Cy5 CD8, PE-Cy7 CD69, PE CD62L, PE-Cy5 CD45RA, PE-Cy7 CD45, FITC CD4, PE CD127, and PE-Cy5 CD25. A second phenotypic study was conducted after stimulating SHP-1-KO and WT T cells with anti-CD3/anti-CD28 Dynabeads (Gibco, USA; #11161D) for 4 h at 37°C in a 5% CO_2

incubator. Subsequently, intracellular cytokine (PE IFN-γ, PE Granzyme B, and PE Perforin) staining was performed on unstimulated SHP-1-KO and WT T cells using Cytofix/Cytoperm™ fixation and permeabilisation solution (BD Biosciences). Fc-blocked single-cell suspensions from mouse HCC tumours were phenotypically analysed for T cells using the same antibodies. Data were processed with FlowJo software after samples were collected using a CytomicsTM FC 500 (BECKMAN COULTER, USA) flow cytometer.

HCC PDX models, H&E staining, TUNEL assay, and IHC staining

HCC patient tumour fragments (25–40 mm^3) were implanted subcutaneously into NCG mice (6–8 weeks old) and passaged to establish patient-derived xenograft (PDX) models, confirmed by histological analysis. PDX model mice were randomised into experimental and control groups. Two methods were employed for immune reconstruction: (1) on the same day that healthy volunteer PBMCs (1×10^7 cells) were injected after tumour fragment implantation, immune reconstruction was considered successful when > 5% human CD45 expression was achieved in the peripheral blood of mouse CD45,[35] treatment commenced when tumours became palpable; (2) injecting PBMCs (5×10^6 cells) when tumours reached ~50 mm^3, followed by edited T cells on day 2.[36] T cells (1×10^6 cells) were administered every 4–6 days, based on literature reports and preliminary experiments that assessed the anti-tumour efficacy of different T cell doses and the incidence of graft-versus-host disease (GVHD) in mice.[10,37] Simvastatin was administered at 5 mg/kg daily during combination therapy. Tumour volume was calculated (1/2 × length × $width^2$), with euthanasia criteria set at 1500 mm^3 or > 25% body weight loss. Apoptosis was assessed via TUNEL assay, and $CD8^+$ cell proportions were analysed by IHC (Anti-CD8 alpha, Servicebio) using ImageJ. Flow cytometry and specimen fixation for IHC, H&E staining, TUNEL assay, and whole transcriptome sequencing were performed on the day of sacrifice.

Whole transcriptome sequencing

KO-SHP-1 and WT T cells from three healthy volunteers were sent to Novogene (Beijing, China) for RNA extraction, library building and sequencing, and data analysis. Bulk-RNA-seq was conducted to explore the mechanistic effects of SHP-1 gene KO on T cells. The top 10 DEGs were validated by qPCR, and the primer sequences are shown in Table S1. Tumour samples with intratumoural injections of KO or WT T cells were also subjected to RNA-seq.

The DEGs within the target pathway were analysed for protein interaction using the STRING database (https://cn.string-db.org/), and the protein–protein interaction (PPI) network was constructed using Cytoscape (https://cytoscape.org/) to identify the gene with the largest weight. This gene was selected as a target for combination therapy with T cells. Subsequently, the three databases, including GEPIA (http://gepia.cancer-pku.cn/), Kaplan–Meier Plotter (http://kmplot.com/analysis/), and The Human Protein Atlas (https://www.proteinatlas.org/), were used to analyse whether the expression level of the gene was related to the prognosis of patients with HCC; finally, its efficacy and safety were further observed and verified in a humanised PDX model.

QUANTIFICATION AND STATISTICAL ANALYSIS

Two-tailed unpaired Student's *t*-tests were used to assess differences between two groups, while one-way or two-way analysis of variance (ANOVA) was employed for multiple group comparisons. Kaplan–Meier survival analysis and log-rank tests were used to compare survival outcomes. All statistical calculations were performed using version 8 of GraphPad Prism (Version 8.0, San Diego, California, USA). A p-value ≤ 0.05 was considered statistically significant.